



# Monopod hopping on compliant terrains<sup>☆</sup>

Vasileios Vasilopoulos<sup>a</sup>, Iosif S. Paraskevas<sup>b</sup>, Evangelos G. Papadopoulos<sup>b,\*</sup>

<sup>a</sup> Department of Mechanical Engineering & Applied Mechanics, University of Pennsylvania, Philadelphia, PA, 19104, United States

<sup>b</sup> School of Mechanical Engineering, National Technical University of Athens, 15780 Athens, Greece

## HIGHLIGHTS

- Consideration of the effects of permanent ground deformation and compaction.
- Development of a controller immune to terrain compliance.
- No knowledge requirement of ground parameters.
- Successful tackle of foot slip effects and hard impacts during touchdown.
- The methodology can be extended to other legged robots such as quadrupeds.

## ARTICLE INFO

### Article history:

Received 30 January 2017

Received in revised form 27 November 2017

Accepted 12 January 2018

Available online 31 January 2018

### Keywords:

Legged robots

Hopping robots

Contact modeling

Field robots

Legged robot control

## ABSTRACT

One of the most intriguing research challenges in legged locomotion is robot performance on compliant terrains. The foot-terrain interaction is usually tackled by disregarding some of the effects of ground deformation, like permanent deformation and compaction; however this approach restricts their application to stiff environments. In this work, the foot-terrain interaction is studied, and used in developing a controller immune to terrain compliance. An impact dynamics model is developed, employing a viscoplastic extension of viscoelastic impact models, and used to study the performance of a monopod robot. To include the effects of compliance, a model of the robot that incorporates the description of the foot-terrain interaction is presented. A novel monopod controller immune to ground energy dissipation is developed, which does not require knowledge of ground parameters. The controller adapts to terrain changes quickly, successfully tackles the effects of slip during touchdown, and copes with the problems, which arise during hard impacts, as the terrain becomes stiffer. Simulation results demonstrate the validity of the developed analysis.

© 2018 Elsevier B.V. All rights reserved.

## 1. Introduction

A central goal in the field of legged robotics is the development of machines able to traverse rough terrain, inaccessible to wheeled vehicles. However, such machines are subject to more complex control requirements. The problem is exacerbated when running on terrain with unknown properties. Earlier approaches required a known type of terrain, to be traversed with a statically stable gait, hence simplifying control and stability issues [1]. On the contrary, quadruped robots like Minitaur [2] and IIT's HyQ have recently shown satisfying dynamic response with specific locomotion behaviors, such as bounding or trotting, by imitating animal gait

patterns, on flat [3] or irregular terrains [4]. Other works focused on bipeds running over stair-like terrain [5], while early studies on the RHex platform demonstrated running on rough terrains [6]. However, this robot uses open-loop control, thus forward speed is not controlled tightly. In contrast, the Boston Dynamics' BigDog is capable of performing a variety of locomotion scenarios, such as walking, trotting or bounding, over unknown terrains; however its motion is highly inefficient [7]. On the other hand, StarLETH uses a foot placement strategy with an appropriate distribution of virtual forces among the stance legs, so as to reach and maintain a specific stable gait by rejecting perturbations, such as unexpected obstacles [8]. A similar approach with footstep planning for overcoming significantly rough terrains was used in Boston Dynamics' LittleDog [9]; however, this robot is capable of static walking only.

Despite the emergence of recent works where the ground properties are explicitly considered in the study of hopping [10,11], running [12], walking [13] or tumbling [14], many notable studies

<sup>☆</sup> This work was completed while all authors were with the School of Mechanical Engineering, NTUA, 15780 Athens, Greece.

\* Corresponding author.

E-mail addresses: [vvasilo@seas.upenn.edu](mailto:vvasilo@seas.upenn.edu) (V. Vasilopoulos), [isparas@mail.ntua.gr](mailto:isparas@mail.ntua.gr) (I.S. Paraskevas), [egpapado@central.ntua.gr](mailto:egpapado@central.ntua.gr) (E.G. Papadopoulos).

disregard the importance of foot-terrain interaction. For example, for the two-link monopod, the contact point between the foot and the ground was modeled as a completely stiff revolute joint [15]. A similar assumption led to a controller for a monopod hopping robot, able to control both its speed and height over rough terrain, with a single actuator [16]. In fact, most efforts in the literature consider the terrain as non-deformable. For the MIT Cheetah 2, the authors determine a target ground force profile according to the desired duty cycle and stride duration [17]. Again, the terrain is considered stiff and completely flat. On the other hand, in [18], the case of a rough terrain is considered and a control algorithm for a monopod robot on rough terrain is proposed. However, the robot was considered to possess two actuators, at its prismatic and rotational joints, while the main body apex height, which is crucial when running on rough terrain, was not controlled. Our recent work involved the preliminary development of an energy-based controller for a monopod hopping robot running over compliant terrains using only one actuator [19]. This controller could compensate for ground compliance but neglected friction and phenomena related to hard impacts.

To incorporate the foot-terrain interaction that affects leg motion and energy dissipation, a realistic representation of this interaction is needed. Usually a simplified ground model is chosen, and controllers consider ground effects as disturbances. However, this approach fails in highly deformable environments. Facing compliant terrains as a terramechanics issue [20], a number of researchers make use of Bekker or similar models [21]. Yet, these approaches do not result in an adequate representation of foot-terrain dynamic interaction in all cases. For this reason, other approaches were proposed in works such as [22], where a viscoelastic model is used, or such as [23] where the authors coined the term “*terradynamics*”. The approach in [23] is applicable to the locomotion of the robots examined, but does not include the impact effects, prominent in fast dynamic walking.

In the case of fast dynamic walking, it is reasonable to consider the stance phase as an impact between the toe and the ground. In principle, such impacts can be modeled via three methods [24]: *the stereomechanical theory method, the Finite Element Method (FEM) and the compliant/viscoelastic approach*. The stereomechanical theory does not take into account the entire impact phase but considers it as a discontinuity, missing important impact information. On the other hand, FEM methods are computationally demanding and difficult to use online. The use of compliant (viscoelastic) models seems more appropriate, as different terrains can be described by lumped parameter models with suitable characteristics [25]. However, even in the case of viscoelastic models, permanent deformations are not modeled; for this reason, in other engineering areas, viscoplastic extensions of the viscoelastic models are proposed [26] (the reader is referred to Fig. 3 for a brief comparison between viscoelastic and viscoplastic models). Earlier work employing this approach demonstrated its potential by proving that a viscoplastic model represents more accurately the foot-terrain interaction [27]. Recent works also focus on modeling terrain compliance; however they do not cope with repetitive terrain compressions, while energy loss due to the terrain is neglected [28]. In another work, a similar approach is presented, however again the issue of repetitive loading is not modeled, although their experimental data shows the existence of this issue during stance [29].

In this paper, legged locomotion and control in the presence of foot-terrain interactions are studied. The adverse effects of terrain deformation during motion are illustrated. A viscoplastic model for impact dynamics is developed, which allows a realistic representation of the behavior of fast dynamic walking on compliant terrains. Using gait feedback, a new controller is developed, able to maintain desired apex height and speed with a single actuator. Preliminary results with an initial version of this controller were

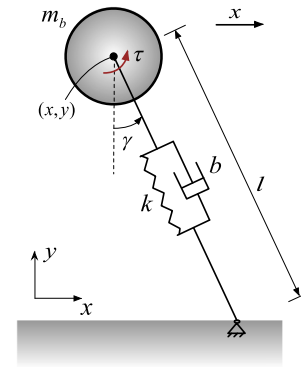


Fig. 1. Monopod simple model.

presented in [19] and extended in [30] for irregular terrains, in [31] for multi-legged robots and even for different gravities in [32]. Here a new version of this controller, capable of retaining the desired motion on terrains with permanent deformations is presented; issues concerning recompressions, friction and extremely stiff terrain are treated also. The importance of these phenomena in hybrid systems is highlighted in a more recent study [33], but no specific control action to cancel them is provided. Simulation results show that the developed controller, called x-MP-II, overcomes terrain variations under different motion scenarios, and achieves gait objectives, still using only one actuator at the robot hip.

## 2. Background on monopod control

*Simple Model (SM).* A hopping monopod robot with a single actuator is considered. The robot is modeled as a body of mass  $m_b$ , with a springy leg, as shown in Fig. 1. The free length of the leg is  $L$ , the stiffness of the linear spring is  $k$ , and the torque applied by the single actuator is  $\tau$ . The angle of the leg with respect to the vertical is  $\gamma$  and its instant length is  $l$ . The energy losses due to viscous friction in the leg prismatic degree of freedom (dof) are modeled by a damping coefficient  $b$ , while the leg mass is considered for this model to be negligible. During stance, and assuming a stiff ground with adequate friction (to avoid slip), the ground interaction can be modeled as a revolute joint. The system variables for both stance and flight phases are taken to be the coordinates of the main body  $x, y$ . The equations of motion for stance (s) are:

$$m_b \ddot{x} + k(L-l)s\gamma - b\dot{s}\gamma = -\tau_s l^{-1} c\gamma \quad (1)$$

$$m_b \ddot{y} + m_b g - k(L-l)c\gamma + b\dot{c}\gamma = -\tau_s l^{-1} s\gamma \quad (2)$$

where  $s\gamma = \sin \gamma$ ,  $c\gamma = \cos \gamma$ , and  $\tau_s$  is the stance actuator torque. During flight (f), the system is assumed to perform a ballistic trajectory, thus the equations of motion become

$$\ddot{x} = 0 \quad (3)$$

$$\ddot{y} = -g \quad (4)$$

During flight, the robot leg is servoed to a desired touchdown angle  $\gamma_{td}$  using a simple proportional derivative (PD) controller. As the robot reaches  $\gamma_{td}$ , its body must not have any residual angular velocity to reduce overshoot. To this end, the control torque applied by the actuator is set by,

$$\tau_f = k_p(\gamma_{td} - \gamma) + k_d(-\dot{\gamma}) \quad (5)$$

where  $k_p$  and  $k_d$  are controller gains.

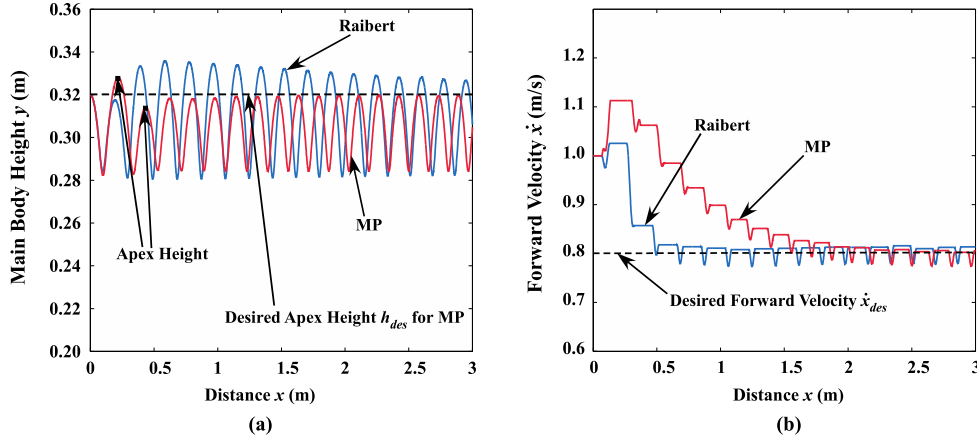


**Fig. 2.** Use of Raibert's Controller and MP on a nondeformable ground: (a) Apex height. (b) Forward velocity. Although Raibert's controller converges faster to the desired forward speed, the MP controller is capable of regulating both the forward speed and the apex height.

Among the various monopod controllers, two characteristic controllers are presented briefly for comparison with the controller developed in this work: Raibert's controller, since it has been used extensively in the legged robotics literature, and the MP controller, as an example of a hopping control law capable of regulating both the apex height and the forward speed.

(a) *Raibert's Controller.* A foot placement algorithm able to regulate the robot forward speed was proposed in [34]. The algorithm uses the assumption that there is a unique foot position for each forward speed, which results in zero net forward acceleration. This foot position is called the "neutral point" and, for each gait  $j$ , it can be determined as the forward displacement  $\Delta x_{f_0}^j$  of the foot with respect to the robot center of mass just before touchdown as follows

$$\Delta x_{f_0}^j = (\dot{x}_{lo}^{j-1} \Delta t_s^{j-1}) / 2 \quad (6)$$

where  $\dot{x}_{lo}^{j-1}$  and  $\Delta t_s^{j-1}$  are the liftoff forward speed and stance duration of gait  $j - 1$  respectively. To accelerate or decelerate the monopod for gait  $j$ , the difference between the actual speed  $\dot{x}_{lo}^{j-1}$  and the desired forward speed  $\dot{x}_{des}$  is used to determine the displacement  $\Delta x_{f_\Delta}^j$  from the neutral point:

$$\Delta x_{f_\Delta}^j = k_x (\dot{x}_{lo}^{j-1} - \dot{x}_{des}) \quad (7)$$

where  $k_x$  is a gain. Combining (6) and (7) yields the algorithm for foot placement  $\Delta x_f^j$  for gait  $j$  as follows

$$\Delta x_f^j = \Delta x_{f_0}^j + \Delta x_{f_\Delta}^j = (\dot{x}_{lo}^{j-1} \Delta t_s^{j-1}) / 2 + k_x (\dot{x}_{lo}^{j-1} - \dot{x}_{des}) \quad (8)$$

Using  $\Delta x_{f_\Delta}^j$ , the desired touchdown angle is found as,

$$\gamma_{td}^j = \sin^{-1} (\Delta x_{f_\Delta}^j L^{-1}) \quad (9)$$

The controller in [34] also includes the means for reaching and maintaining a desired hopping height; however, it requires two actuators, i.e. it relies on the assumption that the leg spring is actuated and that a specific amount of thrust can be delivered during each stance phase. For the monopod used here, the leg spring is not actuated, but behaves instead as a passive element. Therefore, a moderate constant torque is applied in each stance phase to compensate for losses and maintain main body motion. Thus the goal for this controller here will be to maintain a specified forward velocity only.

(b) *MultiPart Controller.* The MultiPart controller (MP) for monopods that can control both the apex height and forward

velocity with a single hip actuator was proposed in [16] and [35]. Controlling apex height is important when running on unknown terrain, allowing the foot to maintain a specific clearance from the ground, thus avoiding obstacles (e.g. rocks). At the end of each stance phase, the controller calculates a desired touchdown angle  $\gamma_{td}$  to achieve the desired apex height and a constant torque  $\tau_s$  applied during stance, to achieve the desired forward speed. To keep the energy consumption to a minimum, the controller requires an estimate of leg compliance and damping, while it applies appropriate actuation to compensate for energy losses.

The desired  $\gamma_{td}$  is found with the use of (2) by making the assumptions: (i) during the stance phase the leg angle  $\gamma$  can be approximated by a linear equation so that:

$$\gamma = \gamma_{td} - \dot{x}_{des} \Delta t L^{-1} \quad (10)$$

where  $\dot{x}_{des}$  and  $\Delta t$  are the desired forward speed and time elapsed since touchdown respectively, (ii) small angle trigonometric approximations are valid and (iii) the actuator torque  $\tau_s$  does not contribute to the body's vertical motion during stance due to (ii). Thus (2) takes the following form:

$$m_b \ddot{y} + b \dot{y} + ky = kL \cos(\gamma_{td} - \dot{x}_{des} \Delta t L^{-1}) - m_b g \quad (11)$$

where the following expressions were used,

$$y = l \cos \gamma \quad (12)$$

$$\dot{y} \approx \dot{l} \cos \gamma \quad (13)$$

With the appropriate initial conditions regarding the beginning of the stance phase and the assumption of a ballistic trajectory during flight, (11) can be integrated twice to yield the desired touchdown angle:

$$\gamma_{td} = f(\text{state at liftoff}, \dot{x}_{des}, h_{des}) \quad (14)$$

where  $h_{des}$  is the desired apex height.

Similarly, the necessary control torque to be applied during the stance phase can be found by linearizing and integrating (1) twice so that,

$$\tau_s = g(\text{state at liftoff}, \dot{x}_{des}, h_{des}, \gamma_{td}) \quad (15)$$

Following the end of the flight phase, the next stance begins, the constant torque  $\tau_s$  is applied, and the cycle repeats itself.

In Fig. 2 the motion of the monopod using the controllers presented earlier on *non-compliant* ground is shown. The parameters of the robot are: body mass  $m_b = 4$  kg, length of the leg  $L = 0.30$  m, spring stiffness  $k = 12,000$  N/m and damping coefficient  $b =$

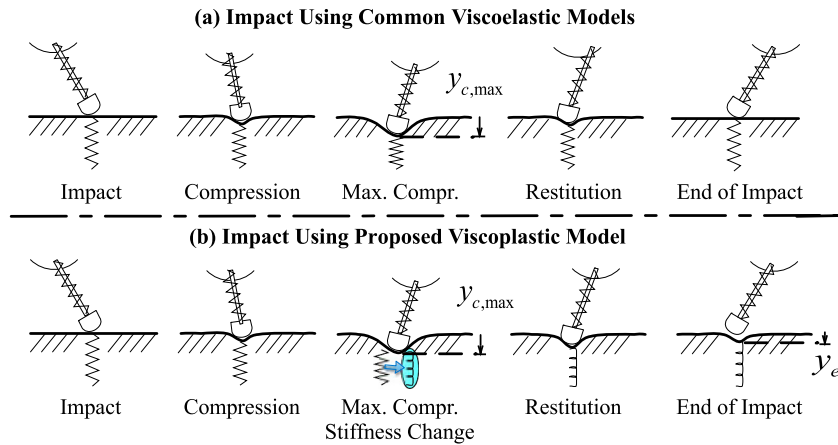


**Fig. 3.** Impact models (a) Standard viscoelastic and (b) Proposed viscoplastic. In contrast to standard viscoelastic models, our viscoplastic model is capable of describing permanent ground deformations.

3 Ns/m. The acceleration of gravity is  $9.81 \text{ m/s}^2$ . The simulations were executed in Matlab using ode23s with absolute and relative tolerance  $10^{-5}$  and  $10^{-4}$  respectively and maximum step  $10^{-4}$ . Regarding the PD controller presented in (5), the values of  $k_p = 150$  and  $k_d = 2.4$  were selected, for the controller to be fast enough to reach  $\gamma_{td}$  before the next touchdown, while avoiding overshooting and undesired oscillations.

Although the controllers presented earlier satisfy the desired gait targets, they both rely on the assumptions of an ideal massless foot and of an interaction with a stiff ground that can be modeled as a revolute joint. It turns out that this is common for most legged robot controllers.

In the subsequent sections, the assumptions of stiff ground and massless foot are dropped, and the corresponding effects on controller performance and gait characteristics are studied. To this end, a realistic terrain model is developed.

### 3. Viscoplastic impact model and friction

**Introduction.** The foot-terrain interaction during running on deformable terrains must be represented realistically. Here the focus is on typical indoor or outdoor terrains, excluding granular media such as sandy terrains, for which interaction forces are of hydrodynamic nature. The main parameters of interest include ground compliance, the depth of the permanent deformation that may occur, and the change of ground characteristics due to repetitive loading at a particular point.

In a terramechanics approach, it is assumed that a wheel or a foot is in touch with the ground for considerable amount of time, or even permanently. This approach cannot be applied in the case of fast dynamic walking, because the stance is practically an impact. It is reasonable to assume that during the foot-terrain interaction, time dependent phenomena, such as creepage, have negligible effect compared to the inertia and interface stiffness or damping effects. However the plastic deformations, which occur to one or both of the interacting bodies, play an important role. A method to incorporate the ground elastoplastic behavior is by using a *viscoplastic* extension of the non-linear viscoelastic models.

According to the viscoelastic theory, a compliant surface can be modeled by a combination of lumped parameter elements, i.e. by springs and dampers. Common impact models include the Kelvin–Voigt (KV) and the Hunt–Crossley (HC) models [25]. As the former introduces non-physical nonlinearities such as non-zero forces at the beginning or the end of an impact, the latter model, which is free of these, will be used as a reference. Additionally, it is the basis for many interesting viscoelastic models found in the literature.

According to the HC model, the interaction force  $F_g$  is,

$$F_g(y_g, \dot{y}_g) = k_g y_g^n + b_g \dot{y}_g^n \quad (16)$$

where  $k_g$  and  $b_g$  are the stiffness and damping coefficients respectively,  $n$  in the case of Hertzian non-adhesive contact is equal to 1.5, and  $y_g$  is the depth of penetration (positive towards the ground). The parameter  $k_g$  represents the equivalent stiffness between the materials that come into contact, in this case the stiffness between the foot and the terrain [36]. Damping is considered as a parameter related to the equivalent stiffness according to [37],

$$b_g = 1.5c_a k_g \quad (17)$$

where  $c_a$  is usually between 0.01–0.5 depending on the materials and the impact velocity [37]. Without affecting the generality of the results, in this work  $c_a = 0.2$  is used.

**Model Rationale.** Existing viscoelastic models implicitly assume that the impact starts and ends (e) at  $y_g = y_e = 0$ , i.e. that no permanent deformation  $y_e$  occurs. However, due to permanent terrain deformation on a nonideal deformable ground, the robot clears the ground at  $y_e > 0$ ; this has an effect on the final spring elongation and the energy lost due to the permanent deformation. In addition, in viscoelastic models, the terrain behavior under repetitive loading or compaction is ignored. This is important when rebounds occur. Hence a model that takes into account such deformations is needed.

Assuming initially a *viscoelastic* model, such as the HC, suppose that a body impacts the ground, as shown in Fig. 3a.

During compression, both the interaction force and depth increase, while the relative to the ground velocity decreases. When the foot velocity is zeroed, i.e.  $\dot{y}_g = 0$ , the maximum compression  $y_{c,max}$  has been reached. Note that generally, the maximum force appears before the maximum compression due to model non-linearity. During restitution, the foot velocity increases, but in the opposite direction, while the depth and the interaction force decrease. The restitution ends when both the depth and the interaction force are zeroed, but in fact this is due to the closed form of the models. The key event characterizing the end of stance is that the interaction force is zeroed, i.e. there is no more contact between the impacting body and the terrain.

Experimental results as for example in [21], reveal that viscoelastic models do not describe accurately terrain deformation. Yet, the strict viscoelastic description of the process can be extended in the case of plastic deformations via appropriate lumped elements to result in a *viscoplastic* description. Here, a model that treats the impact piecewise is developed, as shown in Fig. 3b.

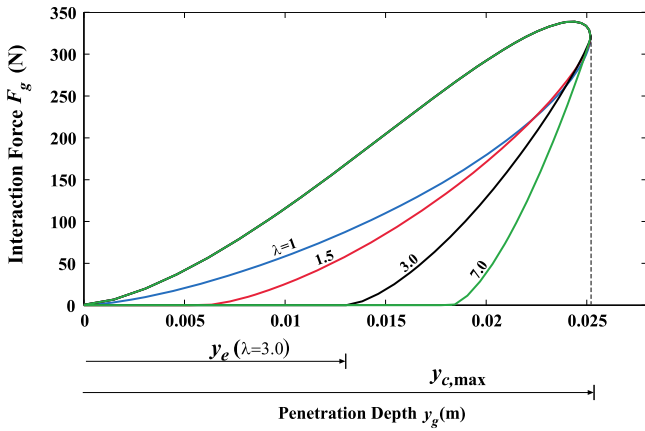


Fig. 4. Impact curves for the proposed impact model (18) for various  $\lambda$ .

According to this model, the compression phase is the same as in the viscoelastic case. During this phase, part of the energy is stored in the (fictitious) spring, which represents the interaction stiffness, another part is dissipated through material internal losses represented by damping  $b_g$ , and the remainder is dissipated during terrain shape deformation, e.g. due to cratering around the impact point or compaction. As restitution is reached, material in the direction of motion has been displaced due to the deformation, and/or the terrain becomes stiffer because of compaction. Also, the interaction spring cannot be extended to its initial length, corresponding to  $y_e = 0$ , but to a shorter length corresponding to a new lower level with  $y_e > 0$  with respect to the undeformed ground. As the interaction force will be zero at this new free length of the spring, it follows that this new fictitious spring is shorter and stiffer. Thus there is memory for the phase between compression and restitution; this memory will be described by a piecewise equation.

*Proposed viscoplastic model.* Based on the above, the interaction force  $F_g$  at instance  $i$  can be described by,

$$F_g^i(y_g, \dot{y}_g) = \begin{cases} F_c^i = (\lambda_c^i k_g + b_g \dot{y}_g) (y_g - y_e^{i-1})^n, & \dot{y}_g \geq 0 \\ F_r^i = (\lambda_r^i k_g + b_g \dot{y}_g) (y_g - y_e^i)^n, & \dot{y}_g < 0 \end{cases} \quad (18)$$

where subscript  $c$  stands for compression,  $r$  for restitution,  $y_e$  is the penetration depth, and the index  $i$  identifies the impact instance, see Fig. 3b. As the terrain inherits characteristics from the previous instance, during successive impacts at the same point, the *Coefficient of Permanent Terrain Deformation*  $\lambda$  is defined in recursive form as,

$$\lambda_c^i = \begin{cases} 1, & i = 1 \\ \lambda_r^{i-1}, & i > 1, i \in \mathbb{N} \end{cases} \quad (19)$$

$$\lambda_r^i = \lambda_r^i(\text{materials, velocity, } i), \quad i \in \mathbb{N}$$

Since the ground spring is stiffer during restitution than in compression,  $\lambda_r^i \geq \lambda_c^i \geq 1$ . The equality  $\lambda_r^i = \lambda_c^i$  holds when the terrain cannot be compressed further; then (18) corresponds to an HC model with the same start and end point. Fig. 4 illustrates the impact force as a function of the penetration depth for various fixed values of  $\lambda$ , as described by (18), in the case of a 1 kg ball falling with zero velocity from a 0.5 m height to a surface with  $k_g = 8 \cdot 10^4$  N/m. Note that with  $\lambda$  increasing, the permanent deformation increases, even though the compression phase is the same. The area under the curve corresponds to interaction losses; these increase with  $\lambda$ .

Parameters for various soils can be obtained easily from the literature, e.g. [21]. However, the experiments yielding these parameters

are of static nature, e.g. using the Bevameter technique, which may not be adequate for dynamic impacts.

Generally, as the same contact area is compressed, it becomes stiffer. Thus after a number of impacts at the same point, its stiffness eventually reaches a critical limit. To model this increasing stiffness, the following function is proposed,

$$\lambda_r^i = 1 + a(i) (1 - e^{-i\beta(i)}), \quad i \in \mathbb{N} \quad (20)$$

where  $a(i)$  and  $\beta(i)$  are functions of the impact instance  $i$  and of the materials and velocity. Note that if  $a(i) = 0$  or  $\beta(i) = 0$ , (18) reduces to the HC model. Parameter  $a$  sets the maximum value of  $\lambda_r^i$ , whereas an increase in  $\beta$  increases the speed to reach this value, i.e. fewer impacts at the same point are needed to reach the critical value.

The final depth  $y_e^i$  after the  $i$ th impact can be calculated by observing that at the maximum compression  $y_{c,\max}^i$  there is force continuity, while the interface velocity is zero, i.e.

$$y_{c,\max}^i \Leftrightarrow F_c^i = F_r^i \quad \text{and} \quad \dot{y}_g = 0 \quad (21)$$

Using (18) and (21) one can deduce

$$y_e^i = y_{c,\max}^i \left( 1 - \sqrt[n]{\lambda_c^i / \lambda_r^i} \right) + y_e^{i-1} \left( \sqrt[n]{\lambda_c^i / \lambda_r^i} \right) \quad (22)$$

where  $y_e^0 = 0$  for consistency.

*Recompressions, rebounds, and hard impacts.* Due to the similarity with a compliant leg, we study the impact behavior of the two-body system in Fig. 5, while it falls vertically. When the lower mass comes into contact with the ground, the direction of the velocity of the system Center of Mass (CoM) is downward. The phases of compression and restitution occur, Fig. 5a and b, and during restitution the lower mass may or may not clear the ground, Fig. 5c. However the upper mass due to its larger inertia and leg compliance, continues its downward motion and thus the forces which are applied on the lower mass by the spring (and damper) and the ground interaction can be equal in magnitude before the direction of the velocity of the system CoM is upward. This will start a "recompression" phase (impact instance  $i + 1$  for this terrain point), Fig. 5d. The process can be repeated a number of times until the robot as a whole clears the terrain and at the same time the direction of the velocity of the system CoM becomes upward; only then the stance is considered over.

The interaction force versus the penetration depth is presented in Fig. 6 for very stiff ground case ( $k_g = 10^6$  N/m), where the upper and lower masses are 4 kg and 0.1 kg respectively, the length of the leg is 0.30 m and the spring stiffness is  $k = 12,000$  N/m. For demonstration purposes, (20) is used with  $a = 0.5$  and  $\beta = 1$ , corresponding to a very stiff terrain, which can be deformed plastically to some small degree. The system falls from a height of 1 cm with zero initial velocity. As can be seen from Fig. 6, a number of compression and restitution phases are observed before the interaction force is zeroed. The remaining compression is about 0.45 mm.

A rebound is completed when the lower mass clears the ground; more than one rebound can occur during a single stance phase. Fig. 7 illustrates this characteristic behavior for two different stance cases. In the first, the lower body undergoes a number of successive recompressions, without liftoff.

In the second, a liftoff of the lower body occurs, without liftoff of the system CoM, which occurs much later. The actual depth penetration as a function of the interaction force depends not only on the materials and the initial impact velocity, but also on the relative stiffness of the system with respect to the ground and the system mass ratio. As a force sensor is used often in legged robots to establish the transition from stance to flight and vice versa, sensor

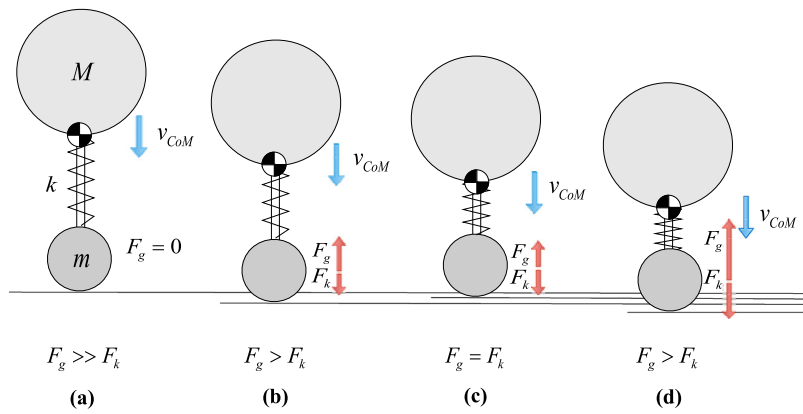


**Fig. 5.** Description of recompression for a falling 2-body system where  $F_g$  is the ground force and  $F_k$  is the spring force: (a) Initial contact, (b) Compression, (c) Restitution and (d) Recompression.

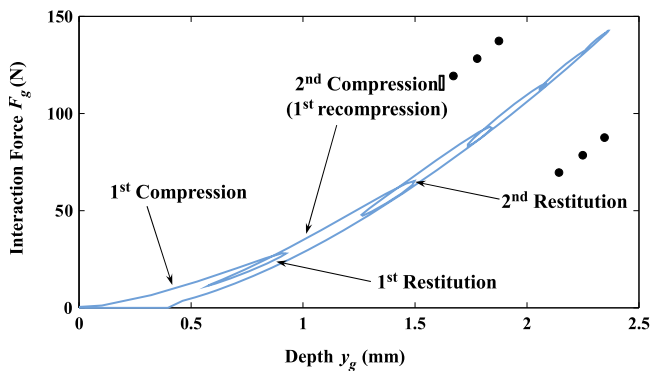


**Fig. 6.** Impact curve for a case with 5 recompressions. Recompressions are shown as inner “loops” in the diagram.

signals can mislead the controller; therefore this behavior must be taken into account in the controller design. Otherwise, flight and stance controllers will be switched on and off very fast, resulting in poor response or even in eventual loss of stability, especially when the impacts are between stiff bodies [38]. Table 1 summarizes the algorithm of the impact model.

**Discussion.** (a) An advantage of the developed model is that it can be used for repetitive loading by increasing the impact instance index  $i$  for a particular contact point. A special case of repetitive loading occurs when the impacting body is a multibody system, such as a legged robot. (b) This model is numerically stiff.

**Table 1**

Summary of the algorithm for the proposed viscoplastic model simulation.

```

<Set initial conditions> For  $k_g$ ,  $b_g$  and  $\lambda_c^i$  from Eq. (19)
<For impact instant  $i$  run> Eq. (18) for  $F_c^i$  until  $\dot{y} = 0$ .
<If  $\dot{y} = 0$ > Keep  $y_c^i$  and calculate  $y_r^i$  from Eq. (22). Set  $\lambda_r^i$  from Eq. (19)
<For impact instant  $i$  run> Eq. (18) for  $F_r^i$ 
  <If  $F_r^i = 0$ > Impact ends
  <Elseif  $F_r^i \neq 0$  and  $\dot{y} = 0$ > Recompression occurs.
    <Set  $\lambda_c^{i+1} = \lambda_r^i$  and start over>
<End>

```

Depending on the complexity of the problem to solve, high accuracy in ODE solvers may be required, (c) The use of the HC model as a basis in (18) is purely a matter of choice; the core idea of the developed model is also applicable to other viscoelastic models, and (d) Proper selection of  $\lambda$  can describe complex phenomena.

**Friction.** The foot response during stance also depends on frictional forces. As the foot touches the ground, depending on the touchdown angle, the velocity and the materials, the foot may slip [25]. Additionally, as the normal component of the interaction force given by (18) near the beginning and the end of the stance phase is low, the same is true for friction. Therefore to properly assess the behavior during stance, a friction description is required. A number of friction models of increasing complexity have been proposed, e.g. see [39]. Here, the classical Static-plus-Coulomb model is employed, as it can produce adequate results with reasonable computations. According to this model the friction

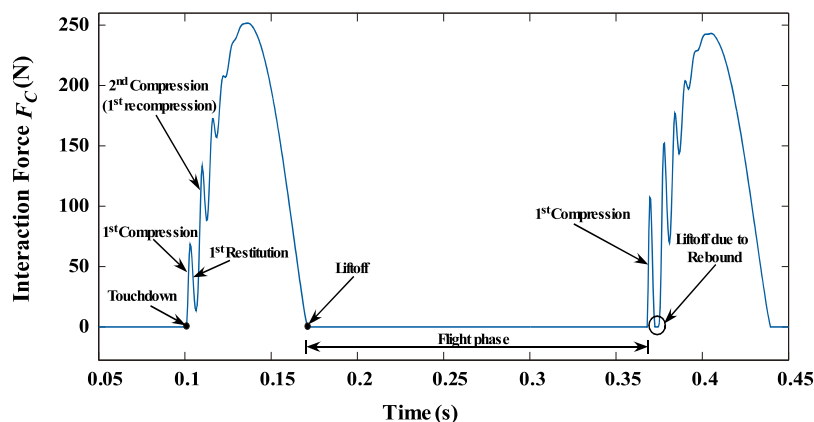


**Fig. 7.** Stance instances with recompressions and rebounds. Rebounds occur when the interaction force is zeroed.

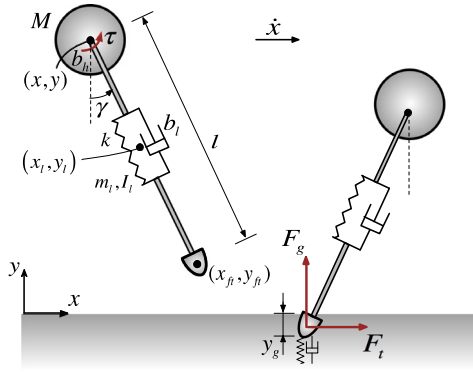


Fig. 8. Detailed Model (DM) of the single-legged robot under examination.

force  $F_t$  is

$$F_t = \begin{cases} -\mu_c F_g \operatorname{sgn} \dot{x}, & \dot{x} \neq 0 \\ -|F_{\parallel}| \operatorname{sgn} F_{\parallel}, & |F_{\parallel}| < \mu_s |F_g|, \dot{x} = 0, \ddot{x} \neq 0 \end{cases} \quad (23)$$

where  $F_g$  is the interaction force from (18) which is normal to the ground tangential plane at the contact point, and  $F_{\parallel}$  is the vectorial sum of all other forces applied, which are parallel to the same tangential plane,  $\mu_c$  is the Coulomb (kinetic) friction coefficient and  $\mu_s$  is the static friction coefficient. Usually, as the depth increases, friction coefficients increase; however here it is assumed that these values do not change during stance.

#### 4. System model and control

To describe the overall response of the robot more accurately, the leg is no longer considered massless. The goal is to make the controller cope with terrain compliance and deformation as well as with friction. In this case, leg mass becomes important, since any ground force is introduced to the robot through its legs. Naturally the leg mass will influence the system behavior during flight as well. A detailed model of the monopod robot that also includes leg inertia and viscous losses on the rotational degree of freedom is developed next.

*Detailed Model (DM).* The model shown in Fig. 8 consists of a mass  $M$  while the leg is considered to be a cylindrical rod of mass  $m_l$  and inertia  $I_l$ . The foot is regarded as the bottom part of that rod and its position  $(x_{ft}, y_{ft})$  can be used to determine the body position  $(x, y)$  by the following kinematic equations

$$x = x_{ft} - l \sin \gamma \quad (24)$$

$$y = y_{ft} + l \cos \gamma \quad (25)$$

On the other hand, the leg Center of Mass  $(x_l, y_l)$  is considered to be located at the middle of the leg, so that,

The energy losses due to viscous friction in the leg prismatic and rotational degree of freedom are introduced through the damping coefficients  $b_l$  and  $b_r$  respectively. The rest of the symbols are the same to those in Section 2.

The ground forces  $F_g$  and  $F_t$  during the stance phase are calculated using (18) and (23) respectively, while during flight  $F_g, F_t = 0$ . It is assumed that: (i) A point contact occurs each time the foot impacts the ground, (ii) bulldozing can be neglected, and (iii) the actuator is torque limited, i.e the actuator maximum continuous current is used to determine the actuator saturation level  $\tau_{\max}$  for continuous operation.

The system variables for both the flight and the stance phase are the leg length  $l$ , the leg angle  $\gamma$  and the coordinates of the foot  $x_{ft}, y_{ft}$ . The equations of motion take the form

$$\mathbf{H}(\mathbf{q}) \ddot{\mathbf{q}} + \mathbf{V}(\mathbf{q}, \dot{\mathbf{q}}) = \mathbf{T} \quad (26)$$

where  $\mathbf{q} = [l \ \gamma \ x_{ft} \ y_{ft}]^T$  and  $\mathbf{H}(\mathbf{q}), \mathbf{V}(\mathbf{q}, \dot{\mathbf{q}})$  and  $\mathbf{T}$  are given in Appendix A. The foot-terrain interaction begins when the foot is about to touch the ground ( $y_{ft} = 0$ ), and terminates when the normal ground force is zeroed ( $F_g = 0$ ). During the foot impact with the ground, the absolute value of the foot coordinate  $y_{ft}$  equals to the depth of penetration.

*Extended MultiPart controller II (x-MP-II).* The MP controller presented in Section 2 depends on robot parameters and is capable of achieving and retaining a desired forward speed and apex height. However, its application is restricted in the case of a monopod robot running on absolutely stiff terrain. To achieve the same goals in the presence of terrain compliance, a new controller called *Extended Multipart controller II* or x-MP-II is developed here. This controller is called at the end of each stance phase and calculates a desired touchdown angle, and a constant torque to be applied during the next stance phase. Also, it compensates for friction and includes a method for maintaining the motion even when non-desired rebounds occur. The controller uses information from a force sensor yielding the ground reaction forces ( $F_t, F_g$ ) and from two encoders that measure the leg angle  $\gamma$  and the leg length  $l$ , and estimates the main body position  $(x, y)$  using the robot dynamic model fused with data from an inertial sensor. With these measurements, the foot position  $(x_{ft}, y_{ft})$  is computed using the kinematic equations (24) and (25).

To develop this controller, first an equivalent mass  $M'$ , spring stiffness  $k'$  and damping coefficient  $b'$  for the system of the robot as described by the DM are calculated. Then, these magnitudes are used in order to relate the behavior of the DM to that of the SM. As the leg mass  $m_l$  is considered small compared to the body mass, the equivalent mass is  $M' = M$ .

To determine an appropriate stiffness  $k'$ , the stance phase of gait  $j-1$  is considered as half the period of a harmonic oscillation with natural frequency  $\omega_s^{j-1}$  thus,

$$\Delta t_s^{j-1} = \pi / \omega_s^{j-1} = \pi \cdot \sqrt{M'/k'} \Rightarrow k' = (\pi / \Delta t_s^{j-1})^2 M' \quad (27)$$

with the stance duration  $\Delta t_s^{j-1}$  given by,

$$\Delta t_s^{j-1} = t_{lo}^{j-1} - t_{td}^{j-1} \quad (28)$$

where  $t_{td}^{j-1}$  and  $t_{lo}^{j-1}$  are the touchdown (td) and liftoff (lo) time instants.

The equivalent damping coefficient,  $b'$ , required by the controller, is calculated taking into account that the terrain is considered to be deformable (d). If the same main body vertical motion were conducted on nondeformable (nd) terrain, the maximum compression of the leg spring would have been

$$\Delta l_{\max}^{j-1} = L - y_{\min}^{j-1} \quad (29)$$

where  $y_{\min}^{j-1}$  is the lowest height of the main body mass. Thus the leg length  $l_{nd}^{j-1}$  during stance is approximated as

$$l_{nd}^{j-1}(t) = L - \Delta l_{\max}^{j-1} \cdot \sin \left[ \omega_s^{j-1} (t - t_{td}^{j-1}) \right] \quad (30)$$

where  $t_{td}^{j-1} \leq t \leq t_{lo}^{j-1}$  and  $\omega_s^{j-1}$  is calculated using (27) and (28).

To determine the equivalent damping coefficient  $b'$ , we proceed as follows. The energy losses at the SM are introduced only through the viscous damping of the leg. There, no energy losses occur during flight as the robot mass performs a ballistic trajectory. Thus, the appropriate damping coefficient  $b'$  to be used in the x-MP-II must

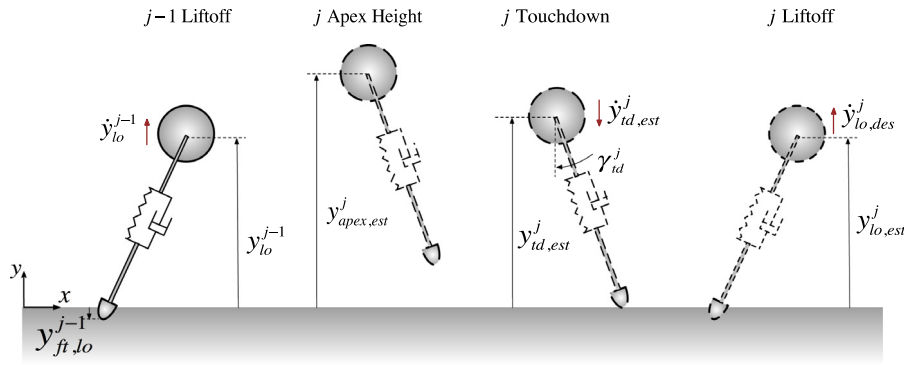


Fig. 9. Predicted (dashed lines) robot motion for an entire stride.

be such as to compensate for all energy losses (leg/hip damping and ground dissipation) that occurred during the stance phase of gait  $j-1$ . Energy losses that occurred during the flight phase will be estimated for use by the torque calculation algorithm. By applying energy conservation and using (30), the following applies

$$b' \int_{t_{td}^{j-1}}^{t_{lo}^{j-1}} (\ddot{h}_{nd}^{j-1})^2 dt = E_{gdis}^{j-1} + E_{damp,s}^{j-1} \quad (31)$$

where  $E_{gdis}^{j-1}$  and  $E_{damp,s}^{j-1}$  are the energy dissipated by the ground, and the energy losses due to viscous friction at the stance phase, respectively. These can be calculated as follows

$$E_{gdis}^{j-1} = \left| \int_{t_{td}^{j-1}}^{t_{lo}^{j-1}} F_g^{j-1} \dot{y}_{ft}^{j-1} dt \right| + \left| \int_{t_{td}^{j-1}}^{t_{lo}^{j-1}} F_t^{j-1} \dot{x}_{ft}^{j-1} dt \right| \quad (32)$$

$$E_{damp,s}^{j-1} = b_l \int_{t_{td}^{j-1}}^{t_{lo}^{j-1}} (\dot{h}^{j-1})^2 dt + b_h \int_{t_{td}^{j-1}}^{t_{lo}^{j-1}} (\dot{\gamma}^{j-1})^2 dt \quad (33)$$

where  $\dot{h}$  and  $\dot{\gamma}$  are the actual rates of leg length and leg angle change respectively.

With the use of (27) and (31),  $k'$  and  $b'$  for the x-MP-II are calculated. With  $M'$ ,  $k'$  and  $b'$  calculated, the x-MP-II calculates the touchdown angle  $\gamma_{td}^j$  and the constant torque to be applied during the stance  $\tau_s^j$ , as follows.

(a) *Desired touchdown angle  $\gamma_{td}^j$* : The variables used in the control algorithm are shown in Fig. 9, where a complete prediction of the robot motion for an entire stride is presented. The main idea for the calculation of the desired touchdown angle  $\gamma_{td}^j$  is to use a prediction of the vertical motion of the robot main body  $y^j(t)$  for the (next) stance phase of gait  $j$  and determine the desired angle  $\gamma_{td}^j$  accordingly, so that a desired main body liftoff height and vertical velocity be reached. In this way, the robot will be allowed to reach the specified apex height, as the main body approximately follows a ballistic trajectory during flight.

Assuming that the duration of the stance phase of gait  $j$  is approximately equal to that of gait  $j-1$ , the vertical response of the robot body during the stance phase of gait  $j$  can be found using (11) with the new equivalent parameters,

$$M' \ddot{y}^j + b' \dot{y}^j + k' y^j = k' L \cos \left( \gamma_{td}^j - \frac{\dot{x}_{des} t}{L} \right) - M' g \quad (34)$$

for  $0 \leq t \leq \Delta t_s^{j-1}$  ( $t = 0$  at touchdown). Eq. (34) is a second order differential equation and can be solved with the following boundary conditions:

$$y^j(0) = y_{td,est}^j = L \cos \gamma_{td}^j \quad (35)$$

$$\dot{y}^j(0) = \dot{y}_{td,est}^j = -\sqrt{2g(y_{apex,est}^j - y_{td,est}^j)} \quad (36)$$

where  $y_{td,est}^j$ ,  $\dot{y}_{td,est}^j$  and  $y_{apex,est}^j$  are the estimated body height at touchdown, the estimated touchdown velocity and the estimated apex height for gait  $j$  respectively. It must be noted that  $y_{apex,est}^j$  can be found from the liftoff velocity  $\dot{y}_{lo}^{j-1}$  and the liftoff height  $y_{lo}^{j-1}$  of gait  $j-1$  assuming a ballistic trajectory during flight as follows,

$$y_{apex,est}^j = y_{lo}^{j-1} + \left( \dot{y}_{lo}^{j-1} \right)^2 (2g)^{-1} \quad (37)$$

Using the boundary conditions (35) and (36), (34) is solved analytically to yield the vertical height prediction

$$y^j(t, \dot{x}_{des}, \gamma_{td}^j) = c_1 e^{a_1 t} \cos(a_2 t) + c_2 e^{a_1 t} \sin(a_2 t) + A \cos \left( \gamma_{td}^j - \frac{\dot{x}_{des} t}{L} \right) + B \cdot \sin \left( \gamma_{td}^j - \frac{\dot{x}_{des} t}{L} \right) - \frac{M' g}{k'} \quad (38)$$

Expressions for the constants  $a_1$ ,  $a_2$ ,  $A$ ,  $B$ ,  $c_1$ ,  $c_2$  are given in Appendix B. Using Fig. 9 and assuming that the depth of ground penetration at the end of the stance phase of gait  $j$  is approximately equal to that of gait  $j-1$ , the body height  $y_{lo,est}^j$  at the end of this stance phase is approximated as,

$$y_{lo,est}^j = y_{ft,lo}^{j-1} + L \cos \left( \gamma_{td}^j - \dot{x}_{des} \Delta t_s^{j-1} L^{-1} \right) \quad (39)$$

Thus, to achieve the desired apex height  $h_{des}$ , the desired vertical velocity  $\dot{y}_{lo,des}^j$  at the end of stance phase of gait  $j$  is

$$\dot{y}_{lo,des}^j = \sqrt{2g(h_{des} - y_{lo,est}^j)} \quad (40)$$

Using (40) and the first time derivative of (38), the following equation must be solved analytically to determine the desired angle  $\gamma_{td}^j$  for a specified desired forward velocity  $\dot{x}_{des}$  and apex height  $h_{des}$

$$\dot{y}^j \left( \Delta t_s^{j-1}, \dot{x}_{des}, \gamma_{td}^j \right) = \dot{y}_{lo,des}^j \left( \Delta t_s^{j-1}, \dot{x}_{des}, h_{des}, \gamma_{td}^j \right) \quad (41)$$

Using Taylor expansion series for  $y_{td,est}^j$  and  $\dot{y}_{lo,des}^j$  presented in (35) and (40) with respect to  $\gamma_{td}^j$ , it can be shown that the desired touchdown angle  $\gamma_{td}^j$  is given by (41) as

$$\gamma_{td}^j = \theta + \cos^{-1}(rR^{-1}) \quad (42)$$

where  $\theta$ ,  $r$  and  $R$  are given in Appendix B. The PD controller presented in (5) is used to position the leg at the desired touchdown angle  $\gamma_{td}^j$  during flight.

(b) *Constant torque  $\tau_s^j$* : The constant torque  $\tau_s^j$  to be applied during the stance phase so as to achieve and maintain the desired

forward speed is calculated such that a desired energy level is secured. The robot is commanded to have height  $h_{des}$  and speed  $\dot{x}_{des}$  at its apex point. It is assumed that at the apex, the leg spring has reached its free length  $L$ , the leg has been positioned already at the desired touchdown angle  $\gamma_{td}^j$  and does not rotate ( $\dot{\gamma} = 0$ ), and the robot body has reached the apex height  $h_{des}$ . Thus, the desired energy level (kinetic and potential) that the system must maintain at gait  $j$  is

$$E_{des}^j = \frac{1}{2} (M + m_l) \dot{x}_{des}^2 + Mgh_{des} + m_l g (h_{des} - 0.5L \cos \gamma_{td}^j) \quad (43)$$

while the liftoff energy of the previous gait  $E_{lo}^{j-1}$  is

$$E_{lo}^{j-1} = \frac{M}{2} \left[ (\dot{x}_{lo}^{j-1})^2 + (\dot{y}_{lo}^{j-1})^2 \right] + \frac{m_l}{2} \left[ (\dot{x}_{l,lo}^{j-1})^2 + (\dot{y}_{l,lo}^{j-1})^2 \right] + \frac{I_l}{2} \dot{\gamma}_{lo}^{j-1} + Mgy_{lo}^{j-1} + m_l g y_{l,lo}^{j-1} + \frac{k}{2} (L - l_{lo}^{j-1})^2 \quad (44)$$

Since the mass of the robot leg  $m_l$  for the DM is considered significantly smaller than  $M$ ,  $E_{des}^j$  and  $E_{lo}^{j-1}$  can be approximated as follows

$$E_{des}^j \approx \frac{1}{2} M \dot{x}_{des}^2 + Mgh_{des} \quad (45)$$

$$E_{lo}^{j-1} \approx \frac{M}{2} \left[ (\dot{x}_{lo}^{j-1})^2 + (\dot{y}_{lo}^{j-1})^2 \right] + \frac{I_l}{2} \dot{\gamma}_{lo}^{j-1} + Mgy_{lo}^{j-1} + \frac{k}{2} (L - l_{lo}^{j-1})^2 \quad (46)$$

The actuator during the stance phase of gait  $j$  must compensate for the losses and maintain the motion, thus the required energy  $E_{m,s}^j$  that it must provide is

$$E_{m,s}^j = (E_{des}^j - E_{lo}^{j-1}) + E_{gdis}^{j-1} + E_{damp}^{j-1} - E_{m,f}^{j-1} \quad (47)$$

where  $E_{m,f}^{j-1}$  is the energy the actuator provided during the flight phase of the gait  $j - 1$ ,  $E_{gdis}^{j-1}$  is the energy dissipated by the ground as shown in (32) and  $E_{damp}^{j-1}$  are the energy losses due to viscous frictions for the whole gait  $j - 1$  so that

$$E_{m,f}^{j-1} = \int_{t_{lo}^{j-2}}^{t_{lo}^{j-1}} \tau^{j-1} \dot{\gamma}^{j-1} dt \quad (48)$$

and

$$E_{damp}^{j-1} = b_l \int_{t_{lo}^{j-2}}^{t_{lo}^{j-1}} (\ddot{l}^{j-1})^2 dt + b_h \int_{t_{lo}^{j-2}}^{t_{lo}^{j-1}} (\dot{\gamma}^{j-1})^2 dt \quad (49)$$

Using (47), the required torque  $\tau_s^j$  is calculated by

$$E_{m,s}^j = \tau_s^j (\gamma_{lo}^{j-1} - \gamma_{td}^{j-1}) \Rightarrow \tau_s^j = E_{m,s}^j (\gamma_{lo}^{j-1} - \gamma_{td}^{j-1})^{-1} \quad (50)$$

If the system had zero losses and the controller achieved the desired motion, then  $E_{des}^j = E_{lo}^{j-1}$  and as predicted by (47) and (50), the motion would reduce to an ideal oscillation with  $\tau_s^j \approx 0$ , i.e. it would correspond to a passive gait.

(c) *Friction compensation.* Except for the calculation of the desired touchdown angle  $\gamma_{td}$  and the constant torque  $\tau_s$  to be applied during the stance phase, a successful controller must be able to tackle the problem of slip in the presence of inadequate friction. Interestingly this occurs mostly at the start of stance and affects the gait characteristics since the foot moves in the horizontal direction and therefore the linear approximation of  $\gamma$  presented in (10) may not apply.

The time interval  $\Delta t_{slip}^{j-1}$  during which the foot may slip at the start of stance phase of gait  $j - 1$  can be found from the time interval

during which  $\dot{x}_{ft,s}^{j-1} \neq 0$ , where  $\dot{x}_{ft,s}^{j-1}$  is the horizontal component of foot velocity during stance. A solution to the slip problem is to command the actuator to exert maximum negative torque for a time interval of  $\Delta t_{slip}^{j-1}$  after touchdown. It must be noted that negative torque corresponds to positive work from the actuator, since in this case the leg moves in the negative direction during stance, which is desired. Using this method,  $\dot{x}_{ft,s}$  is zeroed as fast as possible and the system reaches quickly the desired static friction zone where the foot does not slip in the horizontal direction.

(d) *False liftoff rejection.* Another issue in controller design is related to the rebounds occurring during stance on a very stiff terrain. In such a case, and following a flight phase, the stance may be comprised of several rebounds; then the system loses contact with the ground momentarily, until the inertia of the main body and the leg spring force the foot to impact again. This may happen several times until a proper stance takes place, and if the periods between these rebounds are detected as flight phases by the controller, unstable gaits can result. To tackle this issue, during the contact of the foot with the ground, the x-MP-II compares the contact duration with the estimated stance duration  $\Delta t_s^{j-1}$  equal to half of the system natural period

$$T_n = 2\pi \sqrt{M/k} \quad (51)$$

Obviously, considering the ground effect as well as the viscous losses,  $\Delta t_s^{j-1}$  cannot be less than  $0.5T_n$ . In this way, if  $\Delta t_s^{j-1} \leq 0.5T_n$ , the controller does not apply new  $\gamma_{td}$  or  $\tau_s$ , but it rather waits for the stance phase to be over properly before it applies these. Note that in (51) the stiffness  $k$  was chosen instead of  $k'$  as this criterion is computed before the calculation of  $k'$  in order to determine whether the controller should proceed to its calculations.

*Discussion.* The development of the x-MP-II relies on energy calculations that do not require knowledge of terrain parameters or of a more complex sensor system. For this reason, it is expected that this controller would demonstrate robustness in measurement noise and uncertainties. Also, its application can be easily extended to irregular terrains, by accompanying it with an inclination estimation algorithm, as shown in [30]. Finally, the development of x-MP-II allows its implementation on multi-legged machines; with proper leg coordination, we have already demonstrated that it can successfully generate a pronking gait on a quadrupedal robot [31]. Since the x-MP-II uses data from the previous gait, some approximate initial values are assumed before the first gait is accomplished. The full x-MP-II algorithm is given in Table 2.

## 5. Simulations results

To evaluate the effects of the terrain and examine the behavior of the controller, a set of simulations is run. The equivalent stiffness  $k_g$  between the materials in contact (i.e. foot and ground) is used [36], where the properties of various terrains are taken from [40]. For example, for a rubber foot and granite with Young's modulus  $E = 50$  MPa and  $E = 50$  GPa correspondingly, an equivalent stiffness of  $k_g \approx 327,000$  N/m applies. The friction coefficients  $\mu_s$  and  $\mu_c$  were also selected for various terrains, without affecting the generality of the conclusions [40]. The ground types selected in comparison with the leg stiffness are: *soft* ground, *moderate* ground and *stiff* ground, whose parameters are summarized in Table 3. In all cases, a monopod described by the DM (Fig. 8) is considered. Its parameters are given in Table 4. These parameters were selected to match the values of the hardware platform in [16]. The acceleration of gravity is  $9.81$  m/s<sup>2</sup>. The simulations were performed in Matlab using ode23s with absolute and relative tolerance  $10^{-2}$  and maximum step  $10^{-5}$ . To minimize the zero-crossing arithmetic problems created by the numerical stiffness, the impact was considered over when the interaction

**Table 2**  
Algorithm of the x-MP-II controller.

```

<Calculate  $\Delta t_s^{j-1}$ >
<If  $\Delta t_s^{j-1} \leq 0.5T_n$ > A short-duration flight has occurred
  <Use the former values of  $\gamma_{td}$  and  $\tau_s$  and exit>
<Elseif  $\Delta t_s^{j-1} > 0.5T_n$ > Proceed to the main controller
<Calculate  $\Delta t_{max}^{j-1}$ > Eq. (29)
  <Calculate  $E_{gdis}^{j-1}$  and  $E_{damp,s}^{j-1}$ > Eqs. (32) and (33)
  <Calculate  $k', b'$ > Eqs. (27) and (31)
  <Use  $k', b'$  to calculate  $\gamma_{td}^j$ > Eq. (42)
  <Calculate  $E_{des}^j$  and  $E_{lo}^{j-1}$ > Eqs. (45) and (46)
  <Calculate  $E_{m,f}^j$  and  $E_{damp}^{j-1}$ > Eqs. (48) and (49)
  <Determine  $\tau_s^j$ > Eqs. (47) and (50)
  <Determine the time interval  $\Delta t_{slip}^{j-1}$ >
<End>

```

force between the foot and the terrain was below 5 N, while the foot transition from slip to stick occurred when the foot horizontal velocity was below  $10^{-4}$  m/s. By increasing tolerances, these values can be lower, however this set was selected as it produces both fast and reasonable results.

In Fig. 10, the responses of Raibert's, of the MP, and of the x-MP-II controllers for the defined ground types are compared. The initial conditions are: height  $h_0 = 0.32$  m, forward velocity  $\dot{x}_0 = 1.0$  m/s. The apex height is commanded to change from  $h_{des} = 0.32$  m to 0.34 m at increments of 1 cm, the forward velocity to be  $\dot{x}_{des} = 0.8$  m/s, while the ground is becoming more compliant, in order to make the task more challenging. The figure is divided into three regions according to stiffness. When the ground is stiff, Raibert's and the MP try to achieve the objectives; however they fail to reach the desired velocities. The x-MP-II quickly converges to the desired values. In the moderate ground, Raibert's controller fails to maintain stability. The MP controller on the other hand fails to achieve the desired goals in the moderate and soft ground; as these become more demanding and the terrain compliance more significant, the deviation of the apex height and of the velocity from the desired goals increases. On the contrary, the x-MP-II follows the desired commands.

As expected, Raibert's and MP controllers perform better in stiff terrain than in compliant terrains, i.e.  $k_g \rightarrow (\geq 10^6 \text{ N/m})$ . As compliance increases, they both deviate from the desired commands. This is due to the fact that the mechanics of the impact between the foot and the ground are disregarded; both controllers assume no energy losses occur in stance due to ground compliance. On the other hand, the x-MP-II adapts quickly to each terrain after some transitional steps that depend on ground compliance and actuator saturation level, and maintains its performance independently of the ground.

Although the MP controller fails to achieve its objectives, it is useful to examine the friction profile for an entire gait during the motion of the DM. The profile is shown in Fig. 11, along with the response of the leg angle (a typical normal force profile is shown in Fig. 7). As can be seen in that figure, the leg slips for a short time just after its touchdown and just before its liftoff, where the leg

**Table 4**  
Robot parameters used in simulations.

Parameter	Numerical value
Body mass $M$	4 kg
Leg mass $m_l$	0.5 kg
Leg inertia $I_l$	0.00325 kgm <sup>2</sup>
Leg length $L$	0.3 m
Spring stiffness $k$	12,000 N/m
Leg damping $b_l$	3 Ns/m
Hip damping $b_h$	0.2 Nms
Max torque $\tau_{max}$	4 Nm

angle is large. In this way, the assumption that the foot behaves as a completely stiff revolute joint during each stance phase, on which both Raibert's controller and the MP rely, ceases to apply. This issue is addressed by the x-MP-II, and is successfully tackled resulting in stable motion of the hopping robot. Also, as shown in Fig. 11, our controller achieves the desired result, although the small-angle approximation ceases to apply, despite the fact that recent studies like [41] show the important effect this assumption could have on the control strategy.

Fig. 12 displays the response of the x-MP-II for various terrains where except for different compliances, shape deformation occurs and is described by (20), with  $\alpha(i) = \max \lambda - 1$  ( $\max \lambda$  is included in Fig. 12 for each case) and  $\beta(i) = 1$ ; larger  $\max \lambda$  represents a terrain with deeper permanent deformation, e.g. wet clay. The initial conditions are height  $h_0 = 0.33$  m, forward velocity  $\dot{x}_0 = 1.0$  m/s, with the desired values for apex height and forward velocity shown in Fig. 12. Considering the performance of the x-MP-II with respect to terrain alterations, it can be observed from Fig. 12 that the robot follows the set points for desired main body apex height and forward velocity. In addition, it adapts easily to sudden terrain changes, without being sensitive to permanent terrain deformations.

Deviations during abrupt changes of forward velocity require a few transient gaits until the controller reaches the required energy level and the gaits become stable. The number of these transient gaits increases as the desired values become more demanding or as the terrain compliance increases significantly. This occurs because the actuator is considered to be torque limited; when the constant torque saturation level  $\tau_{max}$  is reached, it can only provide a fixed maximum amount of energy per gait until the actual energy level becomes equal to the system's desired energy level. This is shown in Fig. 13, where the torque applied by the motor is displayed. During the first transient gaits of each terrain type, the torque applied is generally higher and it may reach its saturation level. Apart from that, it can be seen that the torque increases as the ground becomes more compliant. In the inset of Fig. 13, a profile of the torque applied for an entire gait is shown. This profile consists of the PD controller part for the leg placement at the desired touchdown angle, the maximum torque applied for specific time interval after touchdown for slip compensation, and the main torque applied during stance.

## 6. Conclusion

This paper studied legged locomotion in the presence of foot-terrain interactions. The adverse effects of terrain deformation

**Table 3**  
Terrain parameters used in simulations.

Terrain type	Stiffness $k_g$ (N/m)	Static friction coefficient $\mu_s$	Coulomb friction coefficient $\mu_c$
Soft	80,000	0.5	0.4
Moderate	200,000	0.6	0.5
Stiff	400,000	0.7	0.6

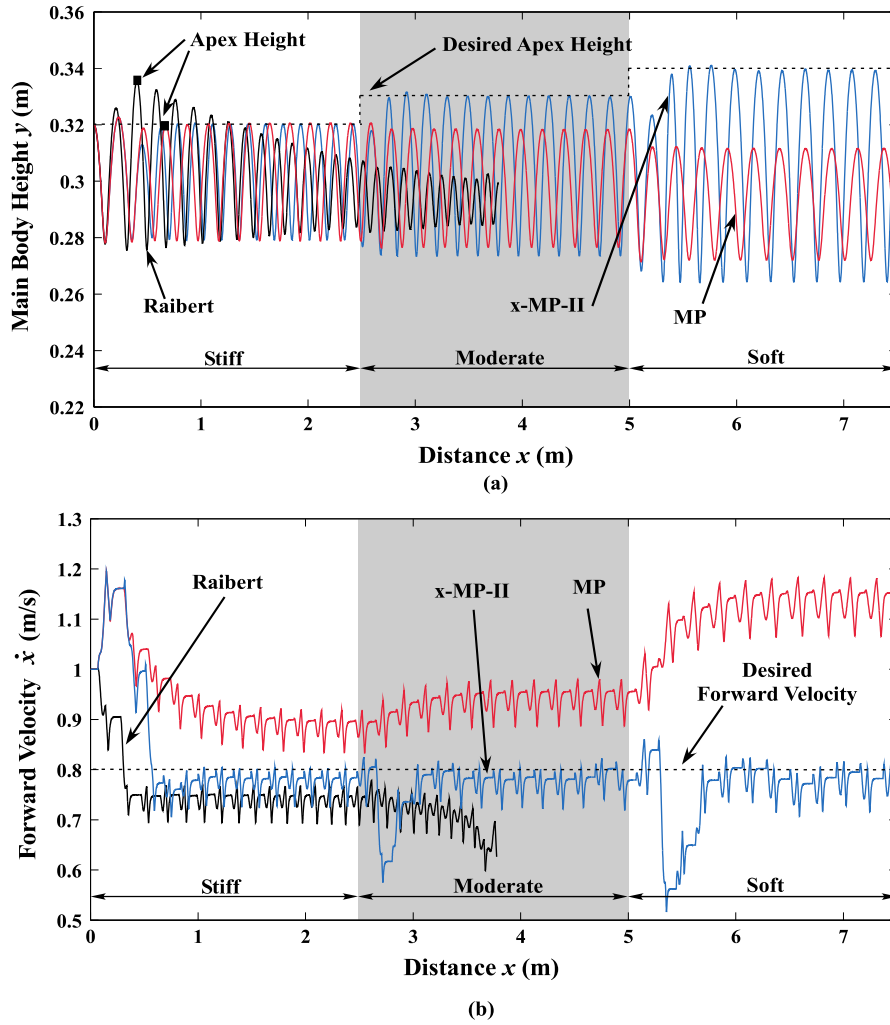


**Fig. 10.** Raibert's Controller, MP & x-MP-II comparison for (a) apex height (b) forward velocity. Raibert's controller fails upon transition to terrain with moderate stiffness and the MP controller fails to achieve the objectives. The x-MP-II, on the other hand, always converges to the desired apex height and forward speed.

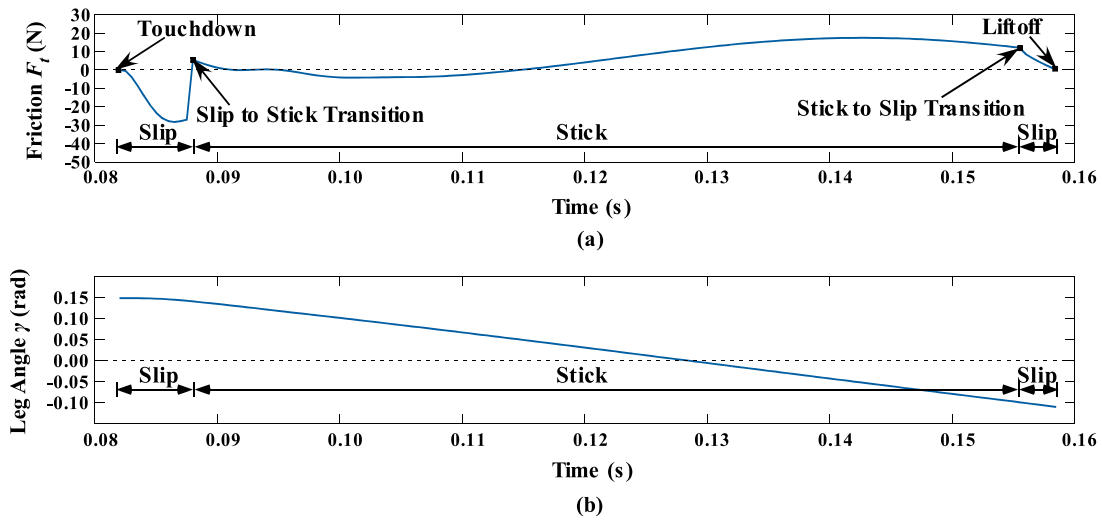


**Fig. 11.** (a) Friction profile and (b) Leg angle during a gait using the MP. Notice the rapid slip-to-stick transition described by our friction model and the almost monotonic evolution of the leg angle during a stance phase.

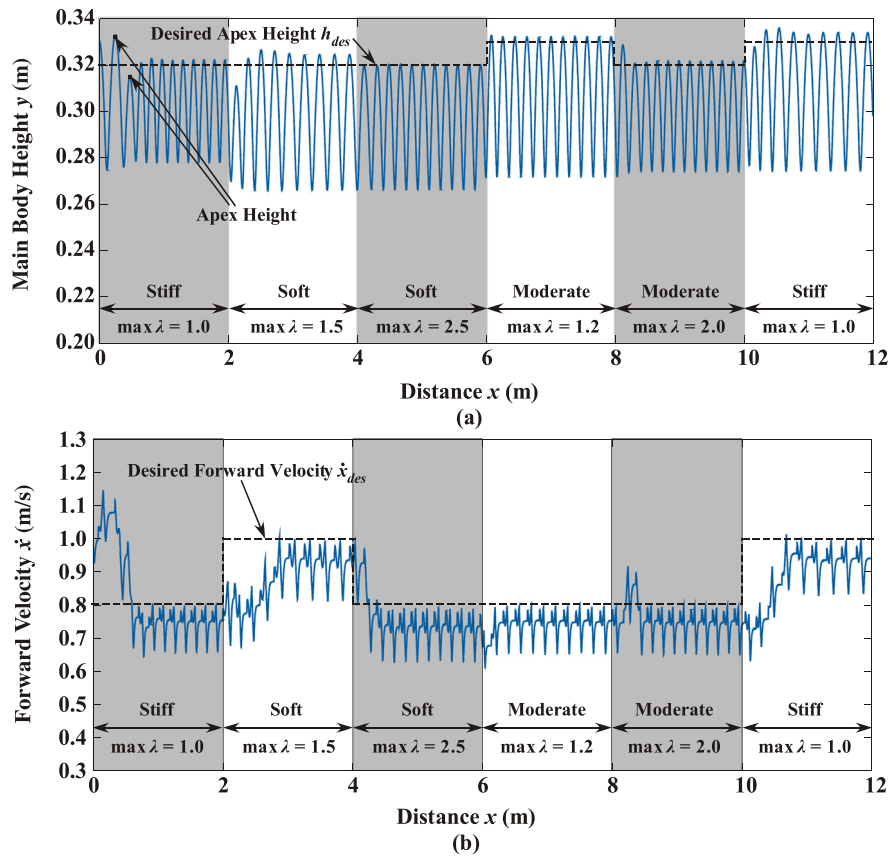


**Fig. 12.** Monopod runs on various terrains using the x-MP-II controller on DM: (a) Apex height and (b) Forward velocity. Our controller always achieves the control objectives on terrains of various characteristics.

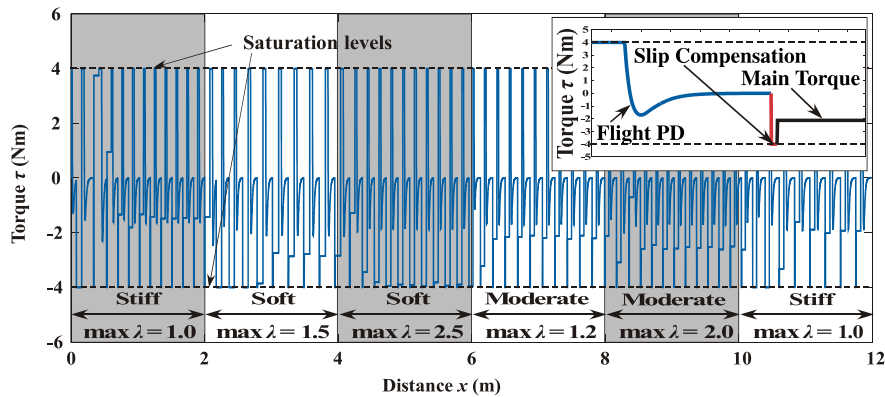


**Fig. 13.** Motor torque during monopod motion. Inset: the applied torque during a gait. Our controller is always successful and, at the same time, never violates the pre-determined torque bounds.

during motion were illustrated. A viscoplastic model for impact dynamics was presented, which allows a realistic representation of the behavior of fast dynamic walking on compliant terrains. Using gait feedback, a new controller was developed by extending results from our previous work, able to maintain desired apex height and speed with a single actuator. The new controller is more robust in retaining the desired motion on terrains with permanent deformations, while it maintains gait stability in the presence of terrain recompressions, low friction, or extremely stiff terrains. Simulation results show that the developed controller overcomes terrain variations under different motion scenarios, and achieves gait objectives, using only one actuator at the robot hip.

## Acknowledgments

The second author acknowledges financial support by the European Union (European Social Fund – ESF) and Greek national funds through the Operational Program “Education and Lifelong Learning” of the National Strategic Reference Framework (NSRF) – Research Funding Program: Heracleitus II. Investing in knowledge society through the European Social Fund. The third author acknowledges financial support by the European Union (European Social Fund – ESF) and Greek funds through the Operational Program “Education and Lifelong Learning” of the National Strategic Reference Framework (NSRF) – Research Program: ARISTEIA:

Reinforcement of the interdisciplinary and/or inter-institutional research and innovation.

## Appendix A

In this Appendix, the matrices  $\mathbf{H}(\mathbf{q})$ ,  $\mathbf{V}(\mathbf{q}, \dot{\mathbf{q}})$  and  $\mathbf{T}$  used in Section 4 for the DM, are presented:

$$\mathbf{H}(\mathbf{q}) = \begin{bmatrix} M_a & 0 & -M_b s \gamma & M_b c \gamma \\ 0 & M_a l^2 + I_l & -M_b l c \gamma & -M_b l s \gamma \\ -M_b s \gamma & -M_b l c \gamma & M + m_l & 0 \\ M_b c \gamma & -M_b l s \gamma & 0 & M + m_l \end{bmatrix} \quad (\text{A.1})$$

$$\mathbf{V}(\mathbf{q}, \dot{\mathbf{q}}) = \begin{bmatrix} b_l \dot{l} - k(L-l) + M_b g c \gamma - M_a l \dot{\gamma}^2 \\ b_h \dot{\gamma} - M_b g l s \gamma + 2M_a l \dot{\gamma} \\ M_b l \dot{\gamma}^2 s \gamma - 2M_b l \dot{\gamma} c \gamma \\ (M + m_l)g - M_b l \dot{\gamma}^2 c \gamma - 2M_b l \dot{\gamma} s \gamma \end{bmatrix} \quad (\text{A.2})$$

$$\mathbf{T} = [0 \quad \tau \quad F_t \quad F_g]^T \quad (\text{A.3})$$

where  $M_a = M + m_l/4$  and  $M_b = M + m_l/2$  are auxiliary variables.

## Appendix B

The constants  $a_1, a_2, A, B, c_1, c_2$  used for the main body vertical height prediction in Section 4 are:

$$a_1 = -b'(2M')^{-1} \quad (\text{B.1})$$

$$a_2 = \sqrt{4M'k' - b'^2}(2M')^{-1} \quad (\text{B.2})$$

$$A = \frac{k'L[k' - M'(\dot{x}_{des})^2 L^{-2}]}{(k' - M'\dot{x}_{des}^2 L^{-2})^2 + (b'\dot{x}_{des} L^{-1})^2} \quad (\text{B.3})$$

$$B = -\frac{k'b'\dot{x}_{des}}{(k' - M'\dot{x}_{des}^2 L^{-2})^2 + (b'\dot{x}_{des} L^{-1})^2} \quad (\text{B.4})$$

$$c_1 = (L - A) \cos \gamma_{td}^j - B \sin \gamma_{td}^j + \frac{M'g}{k'} \quad (\text{B.5})$$

$$c_2 = \left( \dot{\gamma}_{td,est}^j - \frac{A \cdot \dot{x}_{des}}{L} \sin \gamma_{td}^j + \frac{B \cdot \dot{x}_{des}}{L} \cos \gamma_{td}^j - c_1 a_1 \right) a_2^{-1} \quad (\text{B.6})$$

The constants  $\theta, r$  and  $R$  used for the calculation of the desired touchdown angle  $\gamma_{td}^j$  in Section 4 are:

$$\theta = \tan^{-1}(\rho_2/\rho_1) \quad (\text{B.7})$$

$$R = \sqrt{\rho_1^2 + \rho_2^2} \quad (\text{B.8})$$

$$r = \varepsilon_1 + \frac{\delta_2}{a_2} \left( a_1 \frac{M'g}{k'} - \varepsilon_5 \right) - \delta_1 \frac{M'g}{k'} \quad (\text{B.9})$$

where

$$\rho_1 = \delta_1(L - A) + \frac{\delta_2}{a_2} \left[ \frac{B\dot{x}_{des}}{L} - a_1(L - A) + \varepsilon_6 \right] + \delta_3 - \varepsilon_3 \quad (\text{B.10})$$

$$\rho_2 = -B\delta_1 + \frac{\delta_2}{a_2} \left[ -\frac{A\dot{x}_{des}}{L} + a_1 B \right] + \delta_4 - \varepsilon_4 \quad (\text{B.11})$$

and the auxiliary constants  $\delta_1, \delta_2, \delta_3, \delta_4$  and  $\varepsilon_1, \varepsilon_2, \varepsilon_3, \varepsilon_4, \varepsilon_5, \varepsilon_6$  are given by the following equations

$$\delta_1 = a_1 e^{a_1 \Delta t_s^{j-1}} \cos(a_2 \Delta t_s^{j-1}) - a_2 e^{a_1 \Delta t_s^{j-1}} \sin(a_2 \Delta t_s^{j-1}) \quad (\text{B.12})$$

$$\delta_2 = a_1 e^{a_1 \Delta t_s^{j-1}} \sin(a_2 \Delta t_s^{j-1}) + a_2 e^{a_1 \Delta t_s^{j-1}} \cos(a_2 \Delta t_s^{j-1}) \quad (\text{B.13})$$

$$\delta_3 = -\frac{A\dot{x}_{des}}{L} \sin\left(\frac{\dot{x}_{des} \Delta t_s^{j-1}}{L}\right) - \frac{B\dot{x}_{des}}{L} \cos\left(\frac{\dot{x}_{des} \Delta t_s^{j-1}}{L}\right) \quad (\text{B.14})$$

$$\delta_4 = \frac{A\dot{x}_{des}}{L} \cos\left(\frac{\dot{x}_{des} \Delta t_s^{j-1}}{L}\right) - \frac{B\dot{x}_{des}}{L} \sin\left(\frac{\dot{x}_{des} \Delta t_s^{j-1}}{L}\right) \quad (\text{B.15})$$

$$\varepsilon_1 = \sqrt{2g(h_{des} - L - y_{ft,lo}^{j-1})} + \frac{gL}{\sqrt{2g(h_{des} - L - y_{ft,lo}^{j-1})}} \quad (\text{B.16})$$

$$\varepsilon_2 = -\frac{gL}{\sqrt{2g(h_{des} - L - y_{ft,lo}^{j-1})}} \quad (\text{B.17})$$

$$\varepsilon_3 = \varepsilon_2 \cos(\dot{x}_{des} L^{-1} \Delta t_s^{j-1}) \quad (\text{B.18})$$

$$\varepsilon_4 = \varepsilon_2 \sin(\dot{x}_{des} L^{-1} \Delta t_s^{j-1}) \quad (\text{B.19})$$

$$\varepsilon_5 = -\sqrt{2g(y_{apex,est}^j - L)} - \frac{gL}{\sqrt{2g(y_{apex,est}^j - L)}} \quad (\text{B.20})$$

$$\varepsilon_6 = gL \left[ 2g(y_{apex,est}^j - L) \right]^{-1/2} \quad (\text{B.21})$$

## References

- [1] R.B. McGhee, G.I. Iswandhi, Adaptive locomotion of a multilegged robot over rough terrain, *IEEE Trans. Syst. Man Cybern.* 9 (1979) 176–182.
- [2] G. Kenneally, A. De, D.E. Koditschek, Design principles for a family of direct-drive legged robots, *IEEE Robot. Automat. Lett.* (2016).
- [3] I. Havoutis, et al., Quadrupedal trotting with active compliance, *Mechatronics (ICM)*, in: 2013 IEEE International Conference on, pp. 610–616, February 2013.
- [4] S. Bazeille, et al., Quadruped robot trotting over irregular terrain assisted by stereo-vision, *Intell. Serv. Robot.* 7 (2) (2014) 67–77.
- [5] J. Hodgins, Legged robots on rough terrain: Experiments in adjusting step length, in: *IEEE Int. Conf. on Robotics and Automation*, Philadelphia, PA, 1988, pp. 824–826.
- [6] U. Saranlı, M. Buehler, D.E. Koditschek, RHEx: A simple and highly mobile hexapod robot, *Int. J. Robot. Res.* 20 (2001) 616–631.
- [7] M. Buehler, R. Playter, M. Raibert, Robots step outside, in: *Int. Symp. Adaptive Motion of Animals and Machines*, Ilmenau, 2005.
- [8] C. Gehring, et al., Control of dynamic gaits for a quadrupedal robot, in: *IEEE International Conference on Robotics and Automation*, ICRA '13, May 2013, Karlsruhe, Germany, pp. 3287–3292.
- [9] K. Kalakrishnan, et al., Fast robust quadruped locomotion over challenging terrain, in: *IEEE Int. Conf. on Robotics and Automation*, ICRA '10, May 2010, Anchorage, Alaska, USA, pp. 2665–2670.
- [10] J. Nakanishi, A. Radulescu, S. Vijayakumar, Spatio-temporal optimization of multi-phase movements: Dealing with contacts and switching dynamics, in: *IEEE/RSJ Int. Conf. on Intelligent Robots and Systems*, Tokyo, Japan, 2013, pp. 5100–5107.
- [11] M. Rutschmann, B. Satzinger, M. Byl, K. Byl, Nonlinear model predictive control for rough-terrain robot hopping, in: *IEEE/RSJ Int. Conf. on Intelligent Robots and Systems*, 2012, pp. 1859–1864.
- [12] W. Bosworth, J. Whitney, S. Kim, N. Hogan, Robot locomotion on hard and soft ground: Measuring stability and ground properties in situ, in: *IEEE Int. Conf. on Robotics and Automation*, ICRA '16, May 2016, Stockholm, Sweden, pp. 3582–3589.
- [13] C. M. Hubicki, J.J. Aguilar, D.I. Goldman, A.D. Ames, Tractable terrain-aware motion planning on granular media: An Impulsive jumping study, in: *IEEE/RSJ Int. Conf. on Intelligent Robots and Systems*, Daejeon, Korea, 2016, pp. 3887–3892.

- [14] J.V. Albrow, J.E. Bobrow, Motion generation for a tumbling robot using a general contact model, in: IEEE International Conference on Robotics and Automation, ICRA '04, April 2004, New Orleans, pp. 3270–3275.
- [15] M.D. Berkemeier, R.S. Fearing, Sliding and hopping gaits for the underactuated acrobot, *IEEE Trans. Robot. Autom.* 14 (4) (1998) 629–634.
- [16] N. Cherouvim, E. Papadopoulos, Control of hopping speed and height over unknown rough terrain using a single actuator, in: IEEE Int. Conf. on Robotics and Automation, ICRA '09, May 2009, Kobe, Japan, pp. 2743–2748.
- [17] H. Park, et al., Quadruped bounding control with variable duty cycle via vertical impulse scaling, in: IEEE/RSJ Int. Conf. on Int. Robots and Systems, Chicago, Illinois, USA, 2014, pp. 3245–3252.
- [18] S. Faraji, et al., Compliant and adaptive control of a planar monopod hopper in rough terrain, in: IEEE Int. Conf. on Robotics and Automation, ICRA '13, Karlsruhe, Germany, May 2013, pp. 4818–4825.
- [19] V. Vasilopoulos, I.S. Paraskevas, E. Papadopoulos, Compliant terrain legged locomotion using a viscoplastic approach, in: IEEE/RSJ Int. Conf. on Intelligent Robots and Systems, Chicago, Illinois, USA, 2014, pp. 4849–4854.
- [20] L. Ding, et al., Foot-terrain interaction mechanics for legged robots: modeling and experimental validation, *Int. J. Robot. Res.* (2013) 585–1606.
- [21] J.Y. Wong, *Terramechanics and Off-road Vehicle Engineering*, second ed., Elsevier Ltd, 2010.
- [22] A. Wu, H. Geyer, Highly robust running of articulated bipeds in unobserved terrain, in: IEEE/RSJ Int. Conf. on Intelligent Robots and Systems, Chicago, Illinois, USA, 2014, pp. 2558–2565.
- [23] C. Li, T. Zhang, D.I. Goldman, A terradynamics of legged locomotion on granular media, *Science* 339 (6126) (2013) 1408–1412.
- [24] G. Gilardi, I. Sharf, Literature survey of contact dynamics modelling, *Mech. Mach. Theory* 37 (10) (2002) 1213–1239.
- [25] W.J. Stronge, *Impact Mechanics*, Cambridge Univ. Press, 2000.
- [26] A.S. Yigit, A.P. Christoforou, M.A. Majeed, A nonlinear visco-elastoplastic impact model and the coefficient of restitution, *Nonlinear Dynam.* 66 (4) (2011) 509–521.
- [27] I. Koutoulas, et al., Quadruped optimum gaits analysis for planetary exploration, in: 12th Symposium on Advanced Space Technologies in Robotics and Automation, ASTRA '13, ESA, Noordwijk, 2013.
- [28] M. Azad, R. Featherstone, A new nonlinear model of contact normal force, *IEEE Trans. Robot.* 30 (3) (2014) 736–739.
- [29] D. Jacobs, Efficient, stable locomotion in legged robots, (Ph.D. thesis), Dep. of Mech. Engineering, Stanford University, 2012.
- [30] V. Vasilopoulos, I.S. Paraskevas, E.G. Papadopoulos, Control and energy considerations for a hopping monopod on rough compliant terrains, in: IEEE International Conference on Robotics and Automation, ICRA '15, Seattle, WA, USA, May 2015, pp. 4570–4575.
- [31] V. Vasilopoulos, K. Machairas, E.G. Papadopoulos, Quadruped pronking on compliant terrains using a reaction wheel, in: IEEE International Conference on Robotics and Automation, ICRA '16, Stockholm, Sweden, May 2016, pp. 3590–3595.
- [32] V. Vasilopoulos, I.S. Paraskevas, E.G. Papadopoulos, Monopod Hopping on Rough Planetary Environments, in: 13th Symposium on Advanced Space Technologies in Robotics and Automation, ASTRA '15, ESA, ESTEC, Noordwijk, The Netherlands, May 2015.
- [33] A.M. Johnson, S.A. Burden, D.E. Koditschek, A hybrid systems model for simple manipulation and self-manipulation systems, *Int. J. Robot. Res.* 35 (11) (2016).
- [34] M.H. Raibert, *Legged Robots that Balance*, MIT Press, Cambridge, MA, 1986 (19).
- [35] A. Nikolakakis, et al., Implementation of a quadruped robot pronking/ bounding gait using a multipart controller, in: Dynamic Systems and Control Conference, Cambridge, MA, USA, 2010.
- [36] K.L. Johnson, *Contact Mechanics*, Cambridge Univ. Press, 1977.
- [37] D.W. Marhefka, D.E. Orin, A compliant contact model with nonlinear damping for simulation of robotic systems, *IEEE Trans. Syst. Man Cybernet. A: Syst. Humans* 29 (6) (1999) 566–572.
- [38] N. Doh, W.K. Chung, Y. Youm, On hard contact force control, in: IEEE/RSJ International Conference on Intelligent Robots and Systems, IROS, Takamatsu, Japan, 2000, pp. 1528–1533.
- [39] E.G. Papadopoulos, G.C. Chasparis, Analysis and model-based control of servomechanisms with friction, *J. Dynam. Syst. Meas. Control* 126 (4) (2004) 911–915.
- [40] <http://www.stanford.edu/~tyzhu/Documents/Some%20Useful%20Numbers.pdf>.
- [41] U. Saranli, et al., Approximate analytic solutions to non-symmetric stance trajectories of the passive spring-loaded inverted pendulum with damping, *Nonlinear Dynam.* 62 (4) (2010) 729–742.



**Vasileios Vasilopoulos** received his Diploma in Mechanical Engineering in 2014 from the National Technical University of Athens (NTUA). Currently, he is a Ph.D. student in the Department of Mechanical Engineering and Applied Mechanics at the University of Pennsylvania, and is affiliated with the GRASP Lab.

His research interests are in the areas of legged robotics, motion planning, and symbolic control of dynamical systems.

He is a Student Member of IEEE, ASME and AMS.



**Iosif S. Paraskevas** received his Diploma in Mechanical Engineering, MS in Automation, and Ph.D. in Mechanical Engineering, in 2005, 2007 and 2015 respectively from the National Technical University of Athens (NTUA).

Currently he is an External Associate of the Control Systems Lab of the Mechanical Engineering School and the Microprocessors Laboratory and Digital Systems Lab of the School of Electrical and Computer Engineering, both of NTUA. He also works as a freelancer Technical Consultant. His research interests are in the areas of space robotics and space technology, robotics, control, modeling of dynamical systems, and of contact/impact dynamics.

He is a member of the Technical Chamber of Greece (TEE), and a Member of IEEE, ASME, AIAA, and HEL.A.S. (the Hellenic Astronomical Society).



**Evangelos Papadopoulos** received his Diploma from the National Technical University of Athens (NTUA) in 1981, and his M.S. and Ph.D. degrees from MIT in 1983 and 1991 respectively, all in Mechanical Engineering. He was an analyst with the Hellenic Navy, Athens, Greece, from 1985 to 1987. In 1991 he joined McGill U. and the Centre for Intelligent Machines (CIM) as an Assistant Professor. Currently, he is a Professor with the Department of Mechanical Engineering at the NTUA.

He teaches courses in the areas of Systems, Controls, Mechatronics and Robotics. His research interests are in the area of robotics, modeling and control of dynamic systems, mechatronics and design. He has published more than 200 technical articles in journals and refereed conference proceedings. He serves as an Associate Editor for the *ASME J. of Dynamic Systems, Measurement and Control*, the *Machine and Mechanism Theory*, the *IEEE Robotics & Automation Letters*, and the *Frontiers in Space Robotics*, while he served as an Associate Editor of the *IEEE Transactions on Robotics*. He is a Fellow of ASME, an Associate Fellow of AIAA, and a Senior Member of IEEE.